Spatiotemporal soil and saprolite moisture dynamics across a semi-arid woody plant gradient

Ryan J. Niemeyer[a,*], Robert Heinse[b], Timothy E. Link[c], Mark S. Seyfried[d], Zion P. Klos[c], and [e]Christopher J. Williams

[a]Civil and Environmental Engineering, University of Washington, Seattle, WA 98195, USA

[b]Plant, Soil and Entomological and Sciences, University of Idaho, Moscow ID USA

[c]College of Natural Resources, University of Idaho, Moscow, ID 83843, USA

[d]USDA-Agricultural Research Service, Northwest Watershed Research Center, Boise, ID 83712, USA

[e]Department of Statistical Science, University of Idaho, Moscow, ID 83843, USA

[*]Correspondence: Ryan Niemeyer, Dept. of Civil and Environmental Engineering, 201 More Hall, University of Washington, Seattle, WA 98195, USA

Financial support was provided by the NSF's IGERT Program (Award 0903479), United States Geological Survey Northwest Climate Science Center Doctoral Fellowship, and by the National Science Foundation's CBET Program (Award 0854553).

Abstract

Woody plant cover has increased 10-fold in many parts of the semi-arid western U.S. Woody plant cover can alter the timing and amount of moisture accessed by plants in the soil and saprolite. To assess spatiotemporal subsurface moisture dynamics over two water years in a snow-dominated western juniper stand we compared moisture dynamics horizontally across a discontinuous canopy, and vertically in soil and saprolite layers. We monitored continuous soil moisture at 15 and 60 cm and conducted periodic electromagnetic induction and electrical resistivity tomography surveys aimed at sensing moisture changes within the root zone and saprolite. Timing of soil moisture dry down at 15 cm was very similar between the canopy and interspace. Conversely, dry down at 60 cm occurred 22 days earlier in the interspace than in the canopy. Changes in soil moisture after discrete rain events were the principal driver of increases in soil moisture. Interspaces with more shrubs showed greater increases in soil moisture but interspaces with few shrubs showed less increases in soil moisture. For the few rain events that were large enough to increase soil moisture at 60 cm, increases in moisture occurred almost exclusively below the canopy. Soil water holding capacity from 0 to 150 cm was a primary driver of areas that were associated with the greatest change in distributed electrical conductivity – an indicator of changes in soil moisture - across the growing season. Vegetation was also correlated with a greater seasonal change in electrical conductivity at these depths. The seasonal change in resistivity suggested soil moisture extraction well into the saprolite, as deep as 12 m below the surface. This change in deep subsurface moisture primarily occurred below medium and large juniper trees. This study reveals how tree roots are both increasing infiltration below their canopy while also transpiring moisture at depths of upwards of 12 m. Information from this

study can help inform our understanding of juniper resilience to drought and the hydrologic impacts of semi-arid land cover change.

1. Introduction

The hydrologic impacts of woody plant encroachment in semi-arid environments such as with western juniper (*Juniperus occidentalis*) expansion into sagebrush ecosystems are poorly understood. Across the western U.S., woodlands have encroached into sagebrush and grassland ecosystems principally due to grazing and fire exclusion (Tausch et al., 1981; Miller et al., 2005; Romme et al., 2009). This has been followed by restoration efforts to remove woody plants (e.g. Bureau of Land Management, 2015). Increases (decreases) in woody plant cover typically decrease (increase) total runoff (Bosch and Hewlett, 1982; Huang et al., 2006; Zégre et al., 2010; Zou et al., 2014; Qiao et al., 2015). However, documented hydrologic responses of woody plant removal are not always consistent in semi-arid areas. For example, in some cases reductions in woody plant cover were found to have a negligible effect on streamflow (Clary et al., 1974; Baker Jr, 1984; Baker Jr and Ffolliott, 2000), to increase streamflow in the case of tree die-off (Guardiola-Claramonte et al., 2011), or conversely in the case of woodland vegetation expansion to also increase streamflow (Wilcox and Huang, 2010). This information leads some to conclude that woody plant removal in semi-arid regions has a negligible impact on streamflow (Hibbert, 1983; Kuhn et al., 2007; Ffolliott and Gottfried, 2012). These uncertainties about woody plant impacts on streamflow have motivated this study that aims to improve our process-based understanding of the subsurface hydrological processes in these systems.

The impact of changes in woody plant cover on subsurface water processes is of particular importance to land managers and downstream users in water-limited semi-arid systems. Soil water dynamics in the near-surface control the phenology and plant productivity in water-limited environments (Loik et al., 2004; Schwinning and Sala, 2004; West et al., 2007; Robinson et al., 2008; Breshears et al., 2009; Penna et al., 2013). Water dynamics in the deep soil and saprolite zones control streamflow generation and groundwater recharge in many systems (Carey et al., 2010; Chauvin et al., 2011; Gabrielli et al., 2012), and provide a moisture pool for some deep rooted semi-arid plants (Breshears et al., 2009; Graham et al., 2010; Schwinning, 2010) including potential hydraulic lift to draw up deep moisture to shallow soil layers (Dawson, 1996; Armas et al., 2010). In the semi-arid western U.S. where soil moisture is a limiting factor in primary productivity, understanding the duration of plant available water is particularly important. For example, an earlier reduction in plant available water can increase vegetation vulnerability to drought (Grieu et al., 1988; Littell et al., 2008). Earlier reductions in plant available water could be realized in future summers which are projected to experience less precipitation and increased temperatures (Abatzoglou and Kolden, 2011), and a decreased snow to rain ratio.

Elucidating how semi-arid woody plants alter subsurface fluxes is often done by comparing subsurface moisture dynamics between vegetation patches and interspace. Semi-arid conifer species are often organized into “patches” with the areas covered by trees being the “patches” embedded in an interspace “matrix” that is dominated by shrubs, grasses, and forbes (Miller et al., 2005). The interspace and canopy are often characterized by differences in nutrient dynamics (Padien and Lajtha, 1992), radiation regime (Breshears et al., 1997b; Martens et al., 2000), throughfall (Eddleman, 1986; Eddleman and Miller, 1991; Taucer, 2006; Owens et al., 2006), and snow deposition (Niemeyer et al., resubmitted). Theoretical work on interactions between tree and interspace vegetation posits that grasses use shallower soil moisture pools earlier in the growing season, whereas woody plants use deeper soil moisture pools later in the growing season (Walker and Noy-Meir, 1982; Peláez et al., 1994; Ryel et al., 2008). Empirical work with periodic or continuous soil moisture measurements have shown that indeed woody plants utilize moisture at shallow and deeper layers while grasses and forbs use shallower moisture (Gifford and Shaw, 1973; Young et al., 1984; Sala et al., 1989; Peláez et al., 1994; Breshears et al., 1997a; Seyfried et al., 2005; Breshears et al., 2009). Previous studies in discontinuous juniper landscapes have observed both earlier depletion of soil water in the grass-dominated interspace compared to juniper patches (Young et al., 1984) and no difference in seasonal soil moisture depletion between the canopy and interspace (Breshears et al., 1997a). To adequately understand differences in drought vulnerability between the shrubs, grasses, and forbes of the interspace and woody vegetation patches, we must adequately characterize spatiotemporal soil moisture dynamics.

Understanding how shifts in woody plant cover change soil moisture in both space and time requires the triangulation of multiple methods. Assessing differences in soil moisture regimes across canopy/interspace patches or woodland/open plots are often limited to a small number of point-scale soil moisture measurements which are often focused on shallow (< 30 cm) soils (Gifford and Shaw, 1973; Young et al., 1984; Breshears et al., 1997a; Seyfried et al., 2005; Robinson et al., 2010; Roundy et al., 2014). This may adequately capture the changes in soil moisture through time in shallow layers but fails to ascertain how these shifts play out across a canopy-interspace continuum or how these changes play out in deeper layers in the subsurface (Robinson et al., 2008). Deep moisture in the soil, saprolite, and bedrock is inherently inaccessible for investigation using direct-contact sensors and hence is difficult to quantify. Emerging geophysical methods such as electrical resistivity tomography (ERT) and electromagnetic induction (EMI) enable the collection of spatially contiguous datasets both horizontally and vertically (Sheets and Hendrickx, 1995; Robinson et al., 2008).

Here we present a study on the differences in subsurface moisture dynamics in space and time between the canopy and interspace. Our approach was to combine high-temporal resolution soil moisture data with periodic spatial geophysical data to sense changes in moisture at depth and across the discontinuous canopy cover. This is the first study in semi-arid woody plant cover to combine both high temporal resolution and broad spatial data to ascertain how canopy and interspace subsurface moisture dynamics differ. Our specific objective is to understand how deeply-rooted trees and shallowly-rooted shrubs differ in their influence on seasonal subsurface moisture dynamics. Results show how these variations in soil and saprolite moisture can differ by depth and time in ways relevant to understanding juniper drought resilience and streamflow generation at the watershed scale.

2. Methods

To assess how the presence of trees affect soil moisture in space and time across a discontinuous canopy, we used a combination of continuous soil moisture and temperature measurements at shallow (< 1 m) soil depths and periodic geophysical measurements starting at peak soil wetness in early spring, continuing throughout the growing season, and ending at the driest point in the water year before the onset of fall precipitation.

2.1 Site Description

This work was carried out at the Reynolds Creek Experimental Watershed (RCEW) and Critical Zone Observatory in the Owyhee Mountains, approximately 80 km southwest of Boise, ID, USA. RCEW is a semi-arid watershed with moderate steepness and snow cover persisting 4 to 6 months of the year. The specific site for this study (Fig. 1, 43.084° N, -116.743° W) was located at 1940 m above m.s.l. The slope and aspect of the site are 26% and 246° respectively.

Geologically, the site overlays vesicular Miocene basalt with columnar jointing that is described further in Ekren et al. (1981). Average annual precipitation at the nearest climate station, located 730 m to the east and 50 m higher in elevation from the study site, was 554 mm. PRISM adjustment (Daly et al., 1994) of monthly precipitation from the climate station from 1962 to 2013 estimated the average annual precipitation at the study site to be 490 mm. Annual precipitation for WY2013 and 2014 was 577 mm and 532 mm, respectively. Average peak snow depth at the site is 110 cm, but for WY2013/14 was 94 cm and 60 cm, respectively. Hourly snow depth, air temperature, relative humidity, and wind speed were measured at the meteorological station at the site with standard methods (see Hanson, 2001 for descriptions). Wind direction at the site is typically from the south by southwest and produces snow drifts on the north or northeast sides of topographic features (Winstral et al., 2009) and vegetation (Niemeyer et al., resubmitted). Plant species present include a mix of western juniper (*Juniperus occidentalis*), low sagebrush (*Artemisia arbuscula*), mountain big sagebrush (*Artemisia tridentata*) as well as several grass and forb species. Our sample plot spanned approximately 1.2 ha and covered low and high density juniper areas to the north and south respectively (Fig. 1). The high (low) density area was defined by greater (lower) juniper stem density and lower (greater) sagebrush stem density.

2.2 Continuous Soil Moisture Measurements

2.2.1 Soil Moisture Data Collection

To analyze changes in soil moisture between the canopy and interspace and through time, we installed continuous soil moisture and temperature sensors in the vicinity of three trees in August of 2012, and one additional tree in June of 2013. The two trees in the high density juniper area were 4.0 m and 3.7 m tall, while the two trees in the low density juniper area were 2.6 m and 3.8 m tall (Fig. 1). Junipers at the study area had a median diameter of 2.9 m (n = 84), therefore with respect to diameter the four trees are representative of the study area. Soil moisture at each tree was monitored by six sensors. Sensors were installed either “under canopy” or in the interspace. Canopy probes were installed at half the distance between the trunk and canopy edge and the interspace probes were located 1 m beyond the canopy edge. Four sensors were installed at 15 cm both under and outside of the canopy on the north and the west or east sides. Sensors were located at either the east or west side of the interspace so as to not have an interspace probe within 1 m of the canopy. Two probes were installed at 60 cm: one in the interspace and one under the canopy, both on the east or west side of the trunk. All east or west probes were 5TM (15 cm probes) or 5TE (60 cm probes) (Decagon Devices, Pullman, WA). All north probes were frequency domain reflectometery (FDR) probes (Stevens Water Monitoring Systems, Portland, OR).

Prior to data analysis we took several steps to pre-process. Soil moisture data were excluded when the soil temperature dropped below 0° C, since probes are only sensitive to liquid water. This only occurred at 15 cm for 3.1% of the time, since in the winter snowpack insulated the soil and prevented freezing. In addition, the collected time-series of soil moisture data had several gaps due to either a) battery or b) sensors failure.

2.2.2 Soil Moisture Data Analysis

To analyze soil moisture data, we compared the change in soil moisture between the interspace and canopy between events and across the entire growing season. This continuous data was collected every 30 minutes, but averaged on an hourly basis prior to analysis. After the FDR probes were installed, the two 15 cm values for the same tree and location (e.g. tree 3 interspace) were averaged during the same time step to analyze differences between location and trees.

To compare rain and snow impacts on soil moisture, we plotted changes in volumetric water content at 15 cm (θ_{15}) and 60 cm (θ_{60}) to snow depth and precipitation (Fig. 2). Snow depth was based on hourly measurements at the meteorological station and hourly time-lapse photos of snow stakes under and outside the canopy at two representative trees (see Niemeyer et al., resubmitted for a more detailed description). All hourly snow depth measurements were averaged within either canopy or interspaces. There was a 54 day period from December 6th, 2013 to January 29th, 2014 when both time-lapse camera batteries failed. The gap in the data was filled based on with the snow depth sensor at the site climate station for the interspace, and with simulated data for the canopy. Snow depth canopy simulations under the juniper canopy were conducted with the Simultaneous Heat and Water (SHAW) model (Flerchinger and Saxton, 1989). See Niemeyer et al. (resubmitted) for more simulation details.

To analyze the degree of influence of location (interspace vs. canopy), hydrometeorology, and antecedent soil moisture conditions, we calculated the change in soil moisture before and after each rain event. Rain events were separated by at least four hours to a) reach a relatively static soil moisture equilibrium and b) not include decreases in the final θ due to evaporation or transpiration. We then calculated the change in θ_{15} ($\Delta\theta_{15}$) and θ_{60} ($\Delta\theta_{60}$) from the rain event. Because the data displayed heteroscedasticity (not shown), we used non-parametric statistical analyses. First, we used Wilcoxon rank-sum test (Wilcoxon and Wilcox, 1964) to compare $\Delta\theta_{15}$ and $\Delta\theta_{60}$ between the tree and interspace. Second, we assessed how $\Delta\theta_{15}$ differed between interspace and canopy measurements paired at the same tree, and how these differences played out across the two sets of trees in the low and high density juniper plots. For this we used a non-parametric factorial ANOVA that does not depend on normality or equality of variance assumptions (McKean and Vidmar, 1994). To further assess how event and location characteristics controlled $\Delta\theta$, we also used a non-parametric regression tree classification (Breiman et al., 1984) based on the following equation:

$$\Delta\theta = P_G + P_{int} + VPD + \theta_{ant} + tree + phase + location \quad (1)$$

where $\Delta\theta$ is $\Delta\theta_{15}$ or $\Delta\theta_{60}$, P_G is the event rain depth, P_{int} is the mean rainfall intensity (mm hr^{-1}), VPD is the average event vapor pressure deficit measured at the climate station (kPa), θ_{ant} is the antecedent θ_{15} or θ_{60} before the event began, tree is which of the four instrumented trees that the probe(s) were located, phase is the juniper classification (low or high juniper density), and location is if the sensor was in the interspace or under the tree. The variables "tree", "phase" and "location" were factor variables in the model.

To assess how the seasonal timing of soil moisture depletion differs between the canopy and interspace, we calculated the day at which θ_{15} and θ_{60} declined to half of the seasonal range ($day_{50\%}$). We estimated $day_{50\%}$as follows:

$$day_{50\%} = [(\max(\theta) - \min(\theta)) \text{ x } 0.5] + \min(\theta) \quad (2)$$

where max(θ) (min(θ)) is the maximum (minimum) θ_{15} and θ_{60} after the snow melted and before the snow first occurred in the fall. Typically it is assumed that halfway between θ at field capacity and θ at plant wilting point is when transpiration begins to decline (Hillel, 1980). Although the maximum θ is likely greater than field capacity, $day_{50\%}$ is still an adequate index for the timing of soil moisture dry down. Due to the small sample size, we used a Wilcoxon rank-sum test to test for difference between the canopy and interspace $day_{50\%}$.

2.3 Distributed Periodic Measurements

To estimate how subsurface moisture changes across heterogeneous tree and interspace cover both laterally and at depth, we employed periodic geophysical measurements through the growing season. First we conducted four EMI surveys to measure changes in near surface moisture through a growing season. Second, to estimate changes in moisture in the soil, saprolite, and weathered bedrock we conducted ERT surveys before the dry season started and at the end of the dry season to measure changes in resistivity that correlate with changes in moisture.

2.3.1 Electromagnetic Induction

2.3.1.1 EMI, Soil, and Rock Data Collection

To estimate soil moisture across the plot encompassing the low and high density juniper areas (Fig. 2), we used EMI. EMI has been used to estimate soil-water properties (Kachanoski and Jong, 1988; Sheets and Hendrickx, 1995; Sherlock and McDonnell, 2003; Corwin and Lesch, 2005; Abdu et al., 2008). EMI can be exploited to ascertain spatial difference in soil texture (Doolittle et al., 1994; Triantafilis et al., 2001; Triantafilis and Lesch, 2005) and changes in soil water content in both space and time (Sherlock and McDonnell, 2003; Abdu et al., 2008; Tromp-van Meerveld and McDonnell, 2009). Changes in soil moisture are based on when measurable differences in soil electrical conductivity occur between wetter and drier soil states. Geo-referenced (SX BlueII, Geneq, Montreal, Canada) soil apparent electrical conductivity (EC_a) was collected with a CMD-1 electromagnetic induction (EMI) conductivity meter (GF Instruments, Brno, Czech Republic). The instrument has both a vertical co-planar ($EMI_{0\text{-}150}$) and horizontal co-planar ($EMI_{0\text{-}75}$) configurations which have approximate depths of exploration of 0 to 75 cm and 0 to 150 cm, respectively (McNeill, 1980). The two depths were chosen to assess surface soil moisture with the $EMI_{0\text{-}75}$ and the entire root zone with the $EMI_{0\text{-}150}$ (Corwin and

Lesch, 2005). The measured EC_a represents an integrated conductivity across the soil depth of exploration (McNeill 1980).

EMI surveys were conducted on four dates during the summer dry down in 2013 (Fig. 2). Thirteen 200 m north-south survey transects spaced 5 m apart were established using a GPS was used to remain on the transect line. When a large tree was encountered, the survey line diverged around it, making effort to remain as close to the linear transect as possible. The instrument was held approximately 8 cm above the ground during the survey. Data underwent a quality control by removing measurements that had atypically high in-phase values observed when the instrument was above conductors such as stabilizing wires for the climate station or metal rods found at the site. Typically only a total of 5 to 15 values for each data set were removed. We transformed the raw EC_a data to a reference 25° C temperature based on the soil temperature at 60 cm for $EMI_{0\text{-}150}$ and 15 cm and 60 cm for $EMI_{0\text{-}75}$. Soil temperatures at 60 cm were averaged across all monitoring points at the four instrumented trees. We used a standard conversion function for this transformation (Sheets and Hendrickx, 1995; Reedy and Scanlon, 2003).

To accurately interpret EC_a data, "soft" subsurface including soil and rock data are required (Sherlock and McDonnell, 2003; Abdu et al., 2008). To link soil physical properties to the EC_a data, we used the spatial statistical algorithm in the ESAP software package to identify eight soil sample locations across the entire EC_a distribution (Lesch et al., 2000). Soil physical properties were characterized down to 90 cm or refusal by sampling at depth ranges of 0 to 10 cm, 10 to 30 cm, 30 to 60 cm, and 60 to 90 cm in April 2014. We were only able to sample to 65 cm for one sample, 72 cm for one sample, and 75 cm for two samples. Particles larger than 2 mm were removed prior to soil analysis (Natural Resources Conservation Service, 1999). After sieving the soil we estimated sand, silt, and clay with the sedimentation method (Gee and Or,

2002) and soil organic matter (SOM) with the loss on ignition method (Nelson et al., 1996) . For each depth we calculated a) water content with the gravimetric method and b) bulk density assuming a particle density of 2.65 g cm^{-3}. We also measured the electrical conductivity of the soil solution (EC_e). Rock content was estimated along transects based on surface rock coverage and subsurface exploration. First, we walked three north-south transects and three east-west transects to characterize the surface rock coverage. This included percent soil cover, percent rock cover, and rock size. We then inferred sub-surface rock content based on a) the surface rock content from the survey and b) subsurface exploration. Subsurface exploration included multiple auger samples both for the eight samples and other samples collected throughout the study period and across the study site. Second, it included four pits with 1.2 m width, 0.8 m length, and 0.8 m depth dug in the high density juniper area to install buried tipping buckets. The rock content was classified into 9 different classes from low to high that ranged from 0 to 35% rock content by volume (Table S1).

In addition to soil and rock data, we also collected tree and snow spatial data. A distributed tree canopy height model was derived from 1 m resolution LiDAR data flown in November of 2007 (Hudak et al., 2002). We conducted the snow survey the winter before the EMI measurements on March 14th, 2013; based on the continuous snow depth sensor at the climate station; this was approximately 15 days after the peak snow water equivalent date, and 67% of peak snow depth. We measured snow depth every 10 m along four 200-m north-south transects that were 20 m apart and spanned the plot. We established a stratified random sampling design by alternating a set of two offset snow depth measurements, either north/south or east/west offsets, 4 m away from each point. To measure snow depth under adjacent trees, we located the closest tree from each initial point, and quantified the canopy radius. On the north and south sides of the tree we measured snow depth at the trunk, half of the radius out from trunk, at the canopy edge, and 1 m outside the canopy edge. If no tree canopy was within a 10 m radius of the initial point, no tree snow depth was measured. To measure snow density and thereby calculate snow water equivalent, we established four snow pits, two in the low and high density juniper areas of the plot. In each pit we measured snow density with a Snowmetrics snow sampler every 10 cm of depth. We calculated an average snow density across the plot to calculate snow water equivalent from depth measurements.

2.3.1.2 Spatial Analysis

We used kriging to interpolate the EC_a, rock, soil, snow, and canopy data to a 2 m resolution. Many environmental variables are positively skewed and require transformation (Goovaerts, 1997). We therefore used a normal-score transformation for EC_a, which is commonly used (Abdu et al., 2008; Tromp-van Meerveld and McDonnell, 2009). We back transformed the normal-score kriged EC_a values for plotting purposes. We used the automap package in R (Hiemstra et al., 2009) to fit the semivariogram with an exponential, spherical, or stein model, depending on which provided the best statistical fit. We calculated water holding capacity (WHC) for each grid by entering the clay and sand content into the Rosetta Pedotransfer Function (Schaap et al., 2001) to generate θ at both field capacity (θ_{fc}) and plant wilting point (θ_{pwp}). WHC was calculated by:

$$WHC = (\theta_{fc} - \theta_{pwp}) \times (1 - rock) \quad (3)$$

where rock is the rock content, which we assume has negligible water storage.

We conducted two statistical analyses with interpolated EC_a data. The first was to assess the controls on EC_a, the second to assess the controls on change in EC_a (ΔEC_a). To evaluate the controls on EC_a, we conducted a univariate regression analysis with EC_a as the dependent variable and θ, rock content, clay content, and sand content as independent variables. The second analysis was to assess the ΔEC_a from May to September, and from August to September. These two time periods were chosen to estimate changes in moisture across the entire season for the former, and during the late season when vegetation was closest to drought stress, for the latter. To assess ΔEC_a we conducted a multiple generalized least squares multiple regression model that includes spatial covariance. We used a generalized least squares model since the errors can be correlated or have unequal variance (Goovaerts, 1997). The model was defined *a priori* as follows:

$$\Delta EC_a = WHC + snow + canopy\_height \quad (4)$$

where canopy_height is the LiDAR-derived canopy height and snow is the interpolated snow water equivalent from the snow surveys. We also conducted a simple linear regression to assess the influence of proximity to vegetation and ΔEC_a.

2.3.2 Electric resistivity tomography and seismic surveys

We conducted ERT surveys in August of 2013 (dry) and May of 2014 (wet) to assess changes in the resistivity related to subsurface moisture seasonal dynamics (Daily et al., 1992; Zhou et al., 2001). The resistivity survey was conducted with a multi-channel ERT system GeoTom MK-RES/IP/SP (GEOLOG2000, Starnberg, Germany) along 4 sequential lines of 25 electrodes for a total transect length of 99 m. We used a combination of Wenner, dipole-dipole, and Schlumberger electrode arrays with 1 m spacing and 10 pseudosection levels. Relative elevation for the topography correction was collected at a centimeter resolution with a total station. Inverse solution reconstruction with the apparent resistivity data was conducted with BERT software (Günther et al., 2006). For inversion, we combined datasets of all three arrays to maximize the accuracy of the reconstruction (Friedel et al., 2006).

To help constrain the depths of soil, saprolite, and weathered bedrock, we conducted a seismic survey in September 2014 along the ERT transect. We used a 96-channel seismograph with 10 Hz geophones at 1 m spacing. A 10 lb sledge hammer and aluminum plate were used for the source and shots were taken every 5 m. Inverse reconstruction of seismic data was constructed with fat-ray wavepath eikonal travel time inversion with Rayfract software package (RAYFRACT, Vancouver, Canada). We assumed 2,000 m sec^{-1} as the boundary between saprolite and moderately weathered bedrock (Begonha and Braga, 2002; Olona et al., 2010; Befus et al., 2011; Holbrook et al., 2013) and 700 m sec^{-1} was a cutoff for soil to saprolite layer (Befus et al., 2011).

We validated the ERT and EMI surveys by comparing the August 2013 ERT and EMI surveys. We averaged the resistivity values from the top 1.5 m of the ERT inversion and the interpolated $EMI_{0\text{-}150}$ data that overlapped the ERT transect.

3. Results

3.1 Soil properties

The soil in the plot was predominantly fine soil with the average clay content of 35% for the top 10 cm and 53% over the entire soil profile (0 to 90 cm). SOM was low at 0.03 g cm^{-3} and 0.02 g cm^{-3} in the top 10 cm and entire soil profile, respectively. Average soil column bulk density was 1.14 g cm^{-3}. These soils are non-saline, having an EC_e of 0.63 dS m^{-1} for the entire soil profile.

3.2 Soil moisture

Figures 2B and 2C show the summer dry down in soil moisture occurring at similar periods in shallow soil but occurring earlier in the interspace than under the juniper canopy at deeper layers. Based on a Wilcoxon rank-sum test, the canopy and interspace $day_{50\%}$ at 15 cm did not statistically differ (p=0.58), as the average $day_{50\%}$ for the canopy and interspace were May 22nd and 27th, respectively. Conversely, at 60 cm the soil moisture dried out later under the tree compared the interspace with a $day_{50\%}$ of July 14th and June 22nd respectively, which were statistically different (p=0.05). This suggests that soil moisture at the surface is evaporated or transpired initially at the surface and deeper moisture pools are used later. It also suggests that interspace deeper soil moisture is used earlier compared to below canopy moisture.

In Figure 3, we see that event size drives $\Delta\theta_{15}$ and $\Delta\theta_{60}$, but varies at different depths and locations (canopy vs. interspace). These data included 148 discernable events over the measurement period when there was no snow on the ground, the total of which was 264 mm of rain. The median event was 4.6 mm, and the upper tertile ranged from 5.9 mm to 29.6 mm. This upper tertile comprised 64% of the total precipitation. A Wilcoxon rank-sum tests between canopy and interspace for $\Delta\theta_{15}$ and $\Delta\theta_{60}$ for this upper P_G tertile was only significant for $\Delta\theta_{60}$ (p=0.02) with $\Delta\theta_{60}$ under the canopy increasing more during rain events than interspace $\Delta\theta_{60}$. Conversely, although the average interspace $\Delta\theta_{15}$ was slightly larger than the canopy $\Delta\theta_{15}$ for events in the upper P_G tertile, the difference was not statistically significant (p=0.52). Despite this result, subtracting the interspace $\Delta\theta_{15}$ from the tree $\Delta\theta_{15}$ and separating the data by the location of the tree (low density and high density juniper areas), Figure 4 reveals a clear difference in moisture dynamics. For small events ($P_G < 5.9$ mm), the difference is negligible. But for larger events ($P_G > 5.9$ mm), tree $\Delta\theta_{15}$ increases more in lower density sagebrush tree-interspace pairs and interspace $\Delta\theta_{15}$ increases more in higher density sagebrush tree-interspace pairs. A non-parametric ANOVA with the difference in interspace and tree $\Delta\theta_{15}$ as the dependent variable, and log P_G and juniper density (low or high) as independent variables, juniper density (p=0.003) and the interaction term (p=0.0009) were statistically significant, but log P_G was not (p=0.18).

The regression tree in Figure 5 confirms the importance of P_G in driving changes in soil moisture, being all three nodes in the $\Delta\theta_{60}$ tree and being the root node in the $\Delta\theta_{15}$ tree (Fig. 5). Increases in soil moisture increase with P_{int}, although this is likely in part related to the fact that P_{int} is linearly correlated with P_G ($R^2 = 0.60$, $p<0.0001$). P_{int} was also retained in the $\Delta\theta_{15}$ tree, although it was a tertiary node and for low $\Delta\theta_{15}$ values. VPD was a secondary node in $\Delta\theta_{15}$ tree for larger $\Delta\theta_{15}$ values, where increasing VPD decreased $\Delta\theta_{15}$.

3.3 Electromagnetic Induction

Figure 6 shows that as the dry season progresses, EC_a gradually decreases in both shallow and deeper layers in the soil. The median for both the $EMI_{0\text{-}75}$ (0 – 75 cm) and $EMI_{0\text{-}150}$ (0 – 150 cm) configurations declined almost by half from May to September, going from 28.6 to 12.0 mS m^{-1} and from 41.5 to 21.6 mS m^{-1}, respectively. The frequency distribution of EC_a further narrowed as the dry season progressed (Fig. 6), with the range from Q1 to Q3 shrinking in both the $EMI_{0\text{-}75}$ from 17.6 to 7.3 mS m^{-1} and in the $EMI_{0\text{-}150}$ from 23.2 mS m^{-1} to 12 mS m^{-1}. Interestingly, despite an 18 mm rain event a day before the September survey, the median, Q1, and Q3 values all decreased across the surveys in both the $EMI_{0\text{-}75}$ and $EMI_{0\text{-}150}$.

Univariate data analysis of EC_a and soil properties showed that the greatest correlation with EC_a was a negative correlation with sand content (R^2=0.92) as shown in Figure 7. EC_a was also positively correlated with θ and clay content (Fig. 6). On the other hand, rock content ranged from 0 to 35% and was not well correlated with EC_a. Considering that soil moisture is the only time-variable property significantly correlated with EC_a, we reason that temporal changes in EC_a are a good predictor of θ changes across the study site.

For the kriged predictor variables, snow water equivalent ranged from 0 cm to 29 cm and the average for pixels with snow was 8.05 cm. WHC in the top 150 cm of the soil ranged from 43.2 cm to 67.2 cm and the mean was 52.0 cm. LiDAR derived vegetation canopy height ranged from 0 to 9.6 m, the mean for pixels greater than 1 m (i.e. pixels with juniper tree present) was 2.8 m.

We used fitted semivariogram models to interpolate EC_a measurements using spherical and stein models (for semivariogram parameters see Table 1). The maps shown in Figure 8 revealed consistently higher EC_a in both $EMI_{0\text{-}75}$ and $EMI_{0\text{-}150}$ in the lower juniper density area of the plot compared to the lower density area. Areas with high conductivity were areas with high clay content and low rock content, and conversely areas with low conductivity were areas with lower clay content and higher rock content. These areas in the southern part of the plot had EC_a lower than 40 mS m^{-1} for the $EMI_{0\text{-}150}$ throughout the study period. The dry stream channel in the middle of the transect for the $EMI_{0\text{-}150}$ shifted from high conductivity (> 100 mS m^{-1}) to low conductivity (< 50 mS m^{-1}).

Comparisons of seasonal changes in EC_a with interpolated snow depth, WHC, and canopy height revealed that WHC was the primary control on ΔEC_a (Table 2). WHC was significant for all models at $p<0.0001$. Canopy height was only significant ($p<0.1$) for the $EMI_{0\text{-}75}$ configuration from May to June and June to August, and the relationship changed from positively correlated to negatively correlated respectively (Table 2). Snow was a significant ($p < 0.05$) variable for the $EMI_{0\text{-}75}$ and ΔEC_a from May to September model.

Comparing ΔEC_a in $EMI_{0\text{-}150}$ to presence of juniper canopy, there was a significant correlation between the canopy height and ΔEC_a from August to September (Fig. 9B, Fig. 10). For the ΔEC_a for the $EMI_{0\text{-}150}$ configuration, the larger the adjacent canopy height was, the greater the ΔEC_a (Fig. 10). Conversely, for the ΔEC_a from May to September, there is no apparent correlation between ΔEC_a and proximity to juniper trees (Fig. 9A).

3.4 Electrical Resistivity Tomography

ERT inversion results are depicted in Figure 11. Along the ERT transect, total canopy coverage (m^2) of all trees within 5 m of the transect per 1 m of transect was greater in the high density juniper area (0 – 35 m) at 5.1 m^2 m^{-1}, compared to 1.7 m^2 m^{-1} in the low density juniper area (60 – 100 m) (Fig. 11A). Furthermore, the total cumulative height of all junipers within 2 m of the transect is 36.3 m in the high density area and 10.7 m in the low density juniper area. The number of sagebrush in the high density area was 0.49 shrubs m^{-2} compared to 1.93 shrubs m^{-2} in the low density area (Fig. 11A).

The seismic data along the same transect revealed a relatively consistent boundary between soil and saprolite and a varying boundary between saprolite and weathered bedrock (Fig. 11B, 12). The depth of the soil ranged from 1.3 m to 3.0 m and was on average 2.1 m in the high density juniper segment of the transect (0 – 35 m) and 1.7 m in the low density juniper segment of the transect (60 – 100 m) (Fig. 11B, 12). The average saprolite and weathered bedrock boundary was 12.9 m (Fig. 11B, 12). This depth below the high density and low density juniper areas, however, was deeper at 15.4 m and 13.4 m respectively. The saprolite and weathered bedrock boundary was shallowest near the dry stream channel (as shallow as 8.0 m).

Time-lapse ERT surveys during wet (May) and dry (August) revealed areas of both low and high resistivity (Fig. 11C,D). Much of the high density juniper area was dominated by low resistivity subsurface values. Conversely, much of the low density juniper area was dominated by high resistivity values. The differences between the wet and the dry ERT surveys produced the most consistent increase in resistivity in the high density (0 – 35 m) juniper area (Fig. 11E,

Fig. 12). Comparing the change in resistivity averaged over the high density juniper area (0 – 35 m) and low density juniper area (60 – 100 m), Figure 13A shows that this relationship persists across all depths measured. The greatest change in resistivity for both low and high density juniper areas was at 4 – 6 m depths (Fig. 13A). Conversely, the lowest changes in resistivity in both areas were in shallow (< 2 m) and deep (> 10 m) depths. Furthermore, we visually see the increases in subsurface resistivity either directly under a clump of medium trees (15 – 35 m) or in proximity to a large juniper tree (0-5 m; 45 – 55 m) (Fig. 12). The presence of trees and change in resistivity is correlated (Fig. 13B), where the subsurface resistivity increase with the presence of more and taller trees. Finally, note that several areas decreased in resistivity between the wet and dry season (Fig. 11E, Fig. 12).

Confirming the high and low resistivity measurements at the surface along the ERT transect were related to water content changes, the EMI_{0-150} interpolated data was well correlated with the top 1.5 m ERT survey, with the slope of -9.9 mS log ohm^{-1}, at $p<0.0001$ and $R^2 = 0.70$. This confirms that the heterogeneities in EC_a and resistivity across the plot are real instead of an instrument error.

4. Discussion

Our expectation was that soil moisture after rain events would increase more in the interspace than under the canopy due to canopy interception loss. Statistically there was no difference in change in shallow moisture ($\Delta\theta_{15}$) after a rain event between the canopy and interspace. However, when this data from the four trees was separated by trees in low and high density juniper areas, for larger events (> 5.9 mm) greater increases in shallow soil moisture was observed in the interspace with more sagebrush (Fig. 4). On the other hand, greater increases in shallow moisture under the canopy than the interspace occurred at the two trees with fewer sagebrush in the interspace (Fig. 4). Furthermore, there were considerably greater increases in deeper soil moisture ($\Delta\theta_{60}$) under the canopy (Fig. 3).

At first, these results are counter-intuitive since juniper canopy storage capacity and interception loss is often high in juniper and assumed to be much greater than grass or sagebrush species as described in the relevant literature (Eddleman and Miller, 1991; Larsen, 1993; Owens et al., 2006; Kuhn et al., 2007; Ffolliott and Gottfried, 2012). What could lead to this counter-intuitive increase in both shallow and deep moisture below the juniper canopies following a rain event? There are three plausible causes: 1) hydrophobicity focusing infiltration and allowing it to reach deeper layers, 2) roots and other preferential flowpaths increasing deep infiltration, and 3) increased infiltration due to focused input from stemflow. In regards to the first possible cause, Madsen et al. (2008) and Robinson et al. (2010) both observed elevated soil hydrophobicity compared to the interspace directly under Utah juniper (*Juniperus osteosperma*) and pinyon pine (*Pinus edulis*). We observed hydrophobicity below several juniper canopies at our site (water drop penetration greater than 1 min, data not shown). Although hydrophobic soils may appear to decrease infiltration locally, they can increase preferential infiltration through cracks in the hydrophobic layer, as suggested by Robinson et al. (2010). These authors observed preferential flow causing deeper infiltration under tree canopies than in the interspace. Furthermore, in other studies surface infiltration was elevated at the base of shrubs or trees compared to the bare interspace (Johnson and Gordon, 1988; Blackburn et al. 1990; Pierini et al., 2014; Zuo et al., 2014). Regarding the second possible cause, roots may facilitate increased infiltration since roots provide “pathways” for water to bypass the soil matrix. Roots have been observed to facilitate deeper infiltration in pinyon and juniper trees (Dasgupta et al., 2006) and in other ecosystems

(Johnson and Lehmann, 2006; Niemeyer et al., 2014). Third, stemflow may result in elevated $\Delta\theta_{60}$. Stemflow concentrates (funnels) water at the tree base and increases preferential flow (Levia and Germer, 2015). However, multiple juniper and pinyon studies have quantified stemflow to be less than 5% of total precipitation (Eddleman and Miller, 1991; Owens et al., 2006).

It is likely that increases in shallow and deep moisture under the canopy after an event are due to increased preferential flow from all three mechanisms. However, Figure 4 does support root facilitation of preferential flow as the primary mechanism. Across the four trees, the trees were relatively the same size, therefore stemflow and hydrophobicity were likely similar. But the primary difference is there are fewer sagebrush in the interspace for tree-interspace pairs where greater increases in below canopy shallow moisture occurred. Figure 14 is a conceptual diagram for potentially how above ground cover influence below ground hydrologic processes. Semi-arid trees intercept more water than the interspace (Eddleman, 1986; Eddleman and Miller, 1991; Taucer, 2006; Owens et al., 2006), and this likely results in a greater amount of total infiltration into the surface of the soil in the interspace. Infiltration to layers deeper than the very shallow subsurface (< 10 cm) is similar between the shrub and interspace, with greater infiltration in interspaces with more sagebrush (Fig. 4). Furthermore, for large events infiltration penetrates to 60 cm in the soil profile under the canopy (Fig. 3B), likely due in part to preferential infiltration pathways along roots, hydrophobic soils, and a small amount of stemflow. Finally, deep tree roots both redistribution of moisture to deeper layers and allow for moisture uptake from deep levels in the saprolite at a later time.

The observation that $day_{50\%}$ in the interspace occurs earlier than under the canopy was also noted by other studies. During two years of soil moisture data collection, Young et al.

(1984) similarly found that soil moisture below juniper trees at 7.5 cm depth was depleted more slowly than in the interspace. Breshears et al. (1998) modeled soil moisture at 2 cm based on soil temperatures and observed drying to occur earlier in the interspace than under the tree canopy. Interestingly, Roundy et al. (2014) in their measurements in the top 30 cm observed more days with a matric potential greater than -1.5 MPa after a juniper removal treatment (chaining and burning) compared to control plots with juniper. However, their study only assessed affects after 3 years of treatment. A longer time period after treatment with greater increases in herbaceous cover may decrease the differences between the control and treatment.

The EMI surveys revealed that soil moisture in the upper 150 cm is principally driven by soil and climate factors. First, the soil sample analysis with EC_a measurements revealed EC_a was negatively correlated with sand content (Fig. 7), a principal determinant in WHC. Second, the multiple generalized least squares analysis of the distributed data revealed that WHC was the principal driver of temporal changes in EC_a (Table 2). In addition, some aspects of the plot drove temporal shifts in EC_a. Similar to Western et al. (1999), EC_a was more variable during the wet season and was more elevated around the intermittent stream channel immediately after the west season (Fig. 8). The observation that there is no clear spatial pattern around tree locations and stand density in ΔEC_a from May to September (Fig. 9A, Table 2) could be that principal differences in soil moisture change is at deeper (> 150 cm) layers (Shaw and Gifford, 1973). This is supported by the result there were only small absolute differences between the tree and interspace $\Delta\theta_{15}$ from May to August (Fig. 2). The ΔEC_a from August to September was correlated with proximity to larger trees (Fig. 9B, Fig. 10), although canopy height was not significant in the generalized least squares model (Table 2). Finally, some areas saw an increase ΔEC_a in the later month (Fig. 9B). Similarly, some areas in the ERT survey saw a decrease in resistivity (Fig. 11E, Fig. 12). This could be due to subsurface ion accumulation (Friedman, 2005). Regardless, temporal patterns in ΔEC_a show clear shifts in seasonal moisture.

It can be inferred from our results that semi-arid woody plants have the potential to transpire subsurface moisture from deep layers, as well as facilitate its transport to those layers for storage. In our study, Figure 12 reveals that there is a greater reduction in subsurface moisture in areas dominated by junipers compared to those dominated by low sagebrush. This is not surprising considering juniper initially develop deep tap roots and then add above ground biomass (Young et al., 1984; Kramer, 1990; Barrett, 2007). Roots are both a mechanism for how moisture moves to deep layers since infiltrating water often follows large roots (Johnson and Lehmann, 2006; Niemeyer et al., 2014) and a mechanism for how moisture can be stored for later transpiration from those deep layers. There is a call by many to retain any junipers on a landscape that are older than 150 years and pre-date euro-American settlement (Miller et al., 2005). Regardless of reasons for preserving or removing these trees, our study reveals that large juniper trees do take up subsurface moisture both in layers as deep as 12 m (Fig. 12) and potentially laterally beyond their canopy (Fig. 9B).

Our study also demonstrates what other observational field studies have shown, that juniper thrive on rocky soils with low WHC (Miller et al., 2005). Studies of western juniper have observed that during pre-Euroamerican settlement in the western U.S., the trees were predominantly found on rocky ridge tops where fire does not propagate as easily. Likely these areas have lower WHC than soil in the mid-slope and valley and must extract water in the saprolite or weathered bedrock in deeper layers. Our study provides process-based evidence that indeed juniper trees extract water from deeper, non-soil layers. Interpolated WHC data revealed lower WHC in the upper 90 cm of the soil in the dense juniper area than the sparse juniper areas

(Table 2). This suggests that the soil moisture required to sustain the juniper in the dense area must be obtained from deeper layers, both because of lower WHC at the upper 90 cm and because the trees are denser (i.e., increased transpiration demand). The ERT surveys largely corroborated that both large juniper and medium juniper clusters result in extraction of moisture from as deep as 10 m (Fig. 12, Fig. 13B). Deep moisture extraction by juniper means it may be more drought-tolerant than other species (Anderegg et al., 2013).

Based on our results, there is a need to focus on deep moisture pools in addition to shallow soil moisture pools. Most studies of woody plants in semi-arid regions have focused on shallow moisture layers (Breshears et al., 1997a; Robinson et al., 2010; Roundy et al., 2014). Deep moisture is important – often controlling streamflow generation (Carey et al., 2010; Chauvin et al., 2011; Gabrielli et al., 2012) and moderating drought impacts on vegetation (Anderegg et al., 2013). As some have pointed out, the presence or lack of deep moisture storage may determine if changes in semi-arid cover alter streamflow at the watershed scale (Seyfried et al., 2005). Our study revealed shallow soil moisture regimes (i.e. at 15 cm) are quite similar, but deeper layer moisture dynamics are controlled by juniper trees. Future studies should further increase our understanding of how woody plant cover alters deep moisture in different climates and juniper densities. As drought risk and precipitation intensity increases with a changing climate (Abatzoglou and Kolden 2011; Kumar et al., 2012), there is greater need to understand how much deep moisture trees transpire and how this affects streamflow generation and drought resilience in a changing climate.

5. Conclusion

To understand how the presence and absence of individual trees across a landscape alter the hydrologic cycle, our study used both continuous shallow (< 1m) measurements and periodic deep (< 10m) geophysical surveys to assess how subsurface moisture dynamics differ between juniper (canopy) and sagebrush (interspace). Our study shows that western juniper access moisture from as deep as 10 m in the subsurface. It also revealed a counter-intuitive relationship between juniper and infiltration: that soil moisture penetrates deeper and in greater amounts under the canopy than in the interspace. These are first steps in understanding the hydrologic processes that drive changes in streamflow observed in semi-arid woody vegetation studies. Furthermore, this advance in the understanding of ecohydrologic processes can help inform future hydrologic models to better predict how future climate and vegetation changes will impact soil moisture and streamflow. This is especially important considering the shifts in a) vegetation due to future western juniper encroachment (Creutzburg et al., 2015) or removal (e.g. Bureau of Land Management, 2015) or b) shifts in timing, intensity, and phase (rain or snow) of precipitation due to climate change (Kumar et al., 2012).

There still remains a need for future research in understanding the impact of land cover change on subsurface moisture. Since our work was carried out over two years, further research is needed to understand how changes in subsurface moisture differ between sequences of wet to dry years, and if trees consistently access deep moisture pools at timescale longer than the scope of this study. Future research could also elucidate the horizontal subsurface impact of semi-arid woody vegetation, and in particular at what horizontal distances and depths do individual woody plants access moisture, since juniper roots have been found to have lateral roots that extent well past the canopy edge (Barrett, 2007). Despite these knowledge gaps, it is clear that semi-arid trees alter the subsurface moisture regime at depth and substantially impact the terrestrial hydrologic cycle of these systems.

Acknowledgement

The authors wish to thank Rebecca Niemeyer, Lucy Holtsnider, Jim Hoppie, Steve Van Vactor, and Mark Murdock for their help with fieldwork. We thank John Bradford and Travis Nielson for conducting a seismic survey. We thank Ian Leslie and Anita Falen for help with soil sample processing. We thank the Reynolds Creek CZO NSF (EAR 1331872) for their field and data support. This work was funded by the National Science Foundation's IGERT (Award 0903479) and CBET (Award 0854553) programs, and the United States Geological Survey's Northwest Climate Science Center Doctoral Fellowship.

References

Abatzoglou, J.T., Kolden, C.A., 2011. Climate change in western US deserts: potential for increased wildfire and invasive annual grasses. Rangel. Ecol. Manag. 64, 471–478.

Abdu, H., Robinson, D.A., Seyfried, M., Jones, S.B., 2008. Geophysical imaging of watershed subsurface patterns and prediction of soil texture and water holding capacity. Water Resour. Res. 44, W00D18.

Anderegg, L.D., Anderegg, W.R., Berry, J.A., 2013. Not all droughts are created equal: translating meteorological drought into woody plant mortality. Tree Physiol. 33, 672–683.

Armas C., Padilla, F.M., Pugnaire, F.I., Jackson, R.B., 2010. Hydraulic lift and tolerance to salinity of semiarid species: consequences for species interactions. Oecologia. 162, 11–21.

Baker Jr, M.B., 1984. Changes in streamflow in an herbicide-treated pinyon-juniper watershed in Arizona. Water Resour. Res. 20, 1639–1642.

Baker Jr, M.B., Ffolliott, P.F., 2000. Contributions of watershed management research to ecosystem-based management in the Colorado River Basin. Land Steward. 21st Century Contrib. Watershed Manag. Proc. RMRS-P-13 USDA For. Serv. 117–128.

Barrett, H., 2007. Western juniper management: a field guide. Oregon Watershed Enhancement Board.

Befus, K.M., Sheehan, A.F., Leopold, M., Anderson, S.P., Anderson, R.S., 2011. Seismic constraints on critical zone architecture, Boulder Creek watershed, Front Range, Colorado. Vadose Zone J. 10, 915–927.

Begonha, A., Braga, M.S., 2002. Weathering of the Oporto granite: geotechnical and physical properties. Catena. 49, 57–76.

Blackburn, W.H., Pierson, F.B., Seyfried, M.S., 1990. Spatial and temporal influence of soil frost on infiltration and erosion of sagebrush rangelands. Water Resour. Bull. 26, 991–997.

Bosch, J.M., Hewlett, J.D., 1982. A review of catchment experiments to determine the effect of vegetation changes on water yield and evapotranspiration. J. Hydrol. 55, 3–23.

Breiman, L., Friedman, J., Stone, C.J., Olshen, R.A., 1984. Classification and regression trees. CRC press.

Breshears, D.D., Myers, O.B., Johnson, S.R., Meyer, C.W., Martens, S.N., 1997a. Differential Use of Spatially Heterogeneous Soil Moisture by Two Semiarid Woody Species: *Pinus Edulis* and *Juniperus Monosperma*. J. Ecol. 85, 289–299.

Breshears, D.D., Rich, P.M., Barnes, F.J., Campbell, K., 1997b. Overstory-imposed heterogeneity in solar radiation and soil moisture in a semiarid woodland. Ecol. Appl. 7, 1201–1215.

Breshears, D.D., Nyhan, J.W., Heil, C.E., Wilcox, B.P., 1998. Effects of woody plants on microclimate in a semiarid woodland: soil temperature and evaporation in canopy and intercanopy patches. Int. J. Plant Sci. 159, 1010–1017.

Breshears, D.D., Myers, O.B., Barnes, F.J., 2009. Horizontal heterogeneity in the frequency of plant-available water with woodland intercanopy–canopy vegetation patch type rivals that occuring vertically by soil depth. Ecohydrology. 2, 503–519.

Bureau of Land Management, 2015. Notice of Intent To Prepare an Environmental Impact Statement for the Proposed Bruneau-Owyhee SageGrouse Habitat Project, Owyhee County, Idaho.

Carey, S.K., Tetzlaff, D., Seibert, J., Soulsby, C., Buttle, J., Laudon, H., McDonnell, J., McGuire, K., Caissie, D., Shanley, J., Kennedy, M., Devito, K., Pomeroy, J.W., 2010. Inter-comparison of hydro-climatic regimes across northern catchments: synchronicity, resistance and resilience. Hydrol. Process. 24, 3591–3602.

Chauvin, G., Flerchinger, G., Link, T.E., Marks, D., Winstral, A., Seyfried, M., 2011. Long-term water balance and conceptual model of a semi-arid mountainous catchment. J. Hydrol.

Clary, W.P., Baker, M.B., O'Conell, P.F., Johnsen, T.N., Cambell, R.E., 1974. Effects of pinyon-juniper removal on natural resource products and uses in Arizona. USDA–Forest Serv. Res. Pap. RM- 128 Rocky Mt. For. Range Exp. Stn. Ft Collins CO.

Corwin, D.L., Lesch, S.M., 2005. Apparent soil electrical conductivity measurements in agriculture. Comput. Electron. Agric. 46, 11–43.

Creutzburg, M.K., Henderson, E.B., Conklin, D.R., 2015. Climate change and land management impact rangeland condition and sage-grouse habitat in southeastern Oregon. AIMS Environ. Sci. 2, 203-236.

Daily, W., Ramirez, A., LaBrecque, D., Nitao, J., 1992. Electrical resistivity tomography of vadose water movement. Water Resour. Res. 28, 1429–1442.

Daly, C., Neilson, R.P., Phillips, D.L., 1994. A statistical-topographic model for mapping climatological precipitation over mountainous terrain. J. Appl. Meteorol. 33, 140–158.

Dasgupta, S., Mohanty, B.P., Köhne, J.M., 2006. Impacts of juniper vegetation and karst geology on subsurface flow processes in the Edwards Plateau, Texas. Vadose Zone J. 5, 1076–1085.

Dawson, T.E., 1996. Determining water use by trees and forests from isotopic, energy balance and transpiration analyses: the roles of tree size and hydraulic lift. Tree Physiol. 16, 263–272.

Doolittle, J.A., Sudduth, K.A., Kitchen, N.R., Indorante, S.J., 1994. Estimating depths to claypans using electromagnetic induction methods. J. Soil Water Conserv. 49, 572–575.

Eddleman, L.E., 1986. Canopy interception of precipitation. Water Resources Research Institute, Oregon State University.

Eddleman, L.E., Miller, P.M., 1991. Potential impacts of western juniper on the hydrologic cycle. In Proceedings, symposium in ecology and management of riparian shrub communities. 29–31.

Ekren, E.B., McIntyre, D.H., Bennett, E.H., and Malde, H.E., 1981. Geologic map of Owyhee County, Idaho, west of longitude 116 degrees W. U.S. Geological Survey Miscellaneous Investigations Series Map I-1256, 1:125,000.

Ffolliott, P.F., Gottfried, G.J., 2012. Hydrologic processes in the pinyon-juniper woodlands: A literature review. U.S. Department of Agriculture, Forest Service, Rocky Mountain Research Station.

Flerchinger, G., Saxton, K., 1989. Simultaneous heat and water model of a freezing snow-residue-soil system I. Theory and development. Trans ASAE. 32, 565–571.

Friedel, S., Thielen, A., Springman, S.M., 2006. Investigation of a slope endangered by rainfall-induced landslides using 3D resistivity tomography and geotechnical testing. J. Appl. Phys. 60, 100–114.

Friedman, S.E., 2005. Soil properties influencing apparent electrical conductivity: A review. Comput. Electron. Agric. 46, 45–70.

Gabrielli, C.P., McDonnell, J.J., Jarvis, W.T., 2012. The role of bedrock groundwater in rainfall–runoff response at hillslope and catchment scales. J. Hydrol. 450–451, 117–133.

Gee, G.W., Or, D., 2002. Particle-size analysis. In Methods of soil analysis. Part 4, Physical Methods. J.H. Dane and Topp, editors. Soil Science Society of America, Madison, WI. 255–293.

Gifford, G.F., Shaw, C.B., 1973. Soil moisture patterns on two chained pinyon-juniper sites in Utah. J. Range Manag. 26, 436–440.

Goovaerts, P., 1997. Geostatistics for natural resources evaluation. Oxford university press, New York, NY, USA. 512 pp.

Graham, R.C., Rossi, A.M., Hubbert, K.R., 2010. Rock to regolith conversion: Producing hospitable substrates for terrestrial ecosystems. GSA Today. 20, 4–9.

Grieu, P., Guehl, J.M., Aussenac, G., 1988. The effects of soil and atmospheric drought on photosynthesis and stomatal control of gas exchange in three coniferous species. Physiol. Plant. 73, 97–104.

Guardiola-Claramonte, M., Troch, P.A., Breshears, D.D., Huxman, T.E., Switanek, M.B., Durcik, M., Cobb, N.S., 2011. Decreased streamflow in semi-arid basins following drought-induced tree die-off: A counter-intuitive and indirect climate impact on hydrology. J. Hydrol. 406, 225–233.

Günther, T., Rücker, C., Spitzer, K., 2006. Three-dimensional modelling and inversion of DC resistivity data incorporating topography—II. Inversion. Geophys. J. Int. 166, 506–517.

Hanson, C.L., 2001. Long-Term Precipitation Database, Reynolds Creek Experimental Watershed, Idaho, United States. Water Resour. Res. 37, 2831–2834.

Hibbert, A.R., 1983. Water yield improvement potential by vegetation management on western rangelands. Water Resour. Bull. 19, 375–382.

Hiemstra, P.H., Pebesma, E.J., Twenhöfel, C.J., Heuvelink, G.B., 2009. Real-time automatic interpolation of ambient gamma dose rates from the Dutch radioactivity monitoring network. Comput. Geosci. 35, 1711–1721.

Hillel, D., 1980. Fundamentals of Soil Physics. Academic Press, New York, NY, USA. 413 pp.

Holbrook, W.S., Riebe, C.S., Elwaseif, M., Hayes, J.L., Basler-Reeder, K., Harry, D.L., Malazian, A., Dosseto, A., Hartsough, P.C., Hopmans, J.W., 2013. Geophysical constraints on deep weathering and water storage potential in the Southern Sierra Critical Zone Observatory. Earth Surf. Process. Landf. 39, 366–380.

Huang, Y., Wilcox, B.P., Stern, L., Perotto-Baldivieso, H., 2006. Springs on rangelands: runoff dynamics and influence of woody plant cover. Hydrol. Process. 20, 3277–3288.

Hudak, A.T., Lefsky, M.A., Cohen, W.B., Berterretche, M., 2002. Integration of lidar and Landsat ETM+ data for estimating and mapping forest canopy height. Remote Sens. Environ. 82, 397–416.

Johnson, C.W., Gordon, N.D., 1988. Runoff and erosion from rainfall simulator plots on sagebrush rangeland. T. ASABE 31, 421–427.

Johnson, M.S., Lehmann, J., 2006. Double-funneling of trees: Stemflow and root-induced preferential flow. Ecoscience. 13, 324–333.

Kachanoski, R.G., Jong, E., 1988. Scale dependence and the temporal persistence of spatial patterns of soil water storage. Water Resour. Res. 24, 85–91.

Kramer, S., 1990. Development and morphology of juvenile western juniper (*Juniperus occidentalis Hook.*). Oregon State University.

Kuhn, T., Cao, D., George, M., 2007. Juniper removal may not increase overall Klamath River Basin water yields. Calif. Agric. 61, 166–171.

Kumar, M., Wang, R., Link, T.E., 2012. Effects of more extreme precipitation regimes on maximum seasonal snow water equivalent. Geophys. Res. Lett. 39, L20504.

Larsen, R.E., 1993. Interception and water holding capacity of western juniper. Oregon State University.

Lesch, S.M., Rhoades, J.D., Corwin, D.L., 2000. ESAP-95 version 2.01 R. User manual and tutorial guide. Res. Rpt. 146.

Levia, D.F., Germer, S., 2015. A review of stemflow generation dynamics and stemflow-environment interactions in forests and shrublands. Rev. Geophys. 53, 673-714.

Littell, J.S., Peterson, D.L., Tjoelker, M., 2008. Douglas-fir growth in mountain ecosystems: water limits tree growth from stand to region. Ecol. Monogr. 78, 349–368.

Loik, M.E., Breshears, D.D., Lauenroth, W.K., Belnap, J., 2004. A multi-scale perspective of water pulses in dryland ecosystems: climatology and ecohydrology of the western USA. Oecologia 141, 269–281.

Madsen, M.D., Chandler, D.G., Belnap, J., 2008. Spatial gradients in ecohydrologic properties within a pinyon-juniper ecosystem. Ecohydrology 1, 349–360.

Martens, S.N., Breshears, D.D., Meyer, C.W., 2000. Spatial distributions of understory light along the grassland/forest continuum: effects of cover, height, and spatial pattern of tree canopies. Ecol. Model. 126, 79–93.

McKean, J.W. Vidmar, T.J., 1994. A Comparison of Two Rank-Based Methods for the Analysis of Linear Models. Am. Stat. 48, 220–229.

McNeill, J.D., 1980. Electromagnetic terrain conductivity measurement at low induction numbers. Geonics Limited, Ontario, CA.

Miller, R.F., Bates, J.D., Svejcar, T.J., Pierson, F.B., Eddleman, L.E., 2005. Biology, ecology, and management of western juniper (*Juniperus occidentalis*). Corvallis USA Or. State Univ. Agric. Exp. Stn. Tech. Bull.

Natural Resources Conservation Service, 1999. Soil Taxonomy: A Basic System of Soil Classification for Making and Interpreting Soil Surveys. 436. 2nd ed. US Department of Agriculture, Soil Conservation Service, Washington D.C. 869 pp.

Nelson, D.W., Sommers, L.E., Sparks, D.L., Page, A.L., Helmke, P.A., Loeppert, R.H., Soltanpour, P.N., Tabatabai, M.A., Johnston, C.T., Sumner, M.E., others, 1996. Total carbon, organic carbon, and organic matter. Methods Soil Anal. Part 3-Chem. Methods. 961–1010.

Niemeyer, R.J., Fremier, A.K., Heinse, R., Chávez, W., DeClerck, F.A.J., 2014. Woody vegetation increases saturated hydraulic conductivity in dry tropical Nicaragua. Vadose Zone J. 13, 1–11.

Niemeyer, R.J., Link, T.E., Seyfried, M.S., Flerchinger, G.L. Surface water input from snowmelt and rain throughfall in western juniper: Potential impacts of climate change and shifts in semi-arid vegetation. Hydrol. Process. (resubmitted)

Olona, J., Pulgar, J.A., Fernandez-Viejo, G., Lopez-Fernandez, C., Gonzalez-Cortina, J.M., 2010. Weathering variations in a granitic massif and related geotechnical properties through seismic and electrical resistivity methods. Surf. Geophys. 8, 585–599.

Owens, M.K., Lyons, R.K., Alejandro, C.L., 2006. Rainfall partitioning within semiarid juniper communities: effects of event size and canopy cover. Hydrol. Process. 20, 3179–3189.

Padien, D.J., Lajtha, K., 1992. Plant spatial pattern and nutrient distribution in pinyon-juniper woodlands along an elevational gradient in northern New Mexico. Int. J. Plant Sci. 425–433.

Peláez, D.V., Distel, R.A., Bóo, R.M., Elia, O.R., Mayor, M.D., 1994. Water relations between shrubs and grasses in semi-arid Argentina. J. Arid Environ. 27, 71–78.

Penna, D., Brocca, L., Borga, M., Dalla Fontana, G., 2013. Soil moisture temporal stability at different depths on two alpine hillslopes during wet and dry periods. J. Hydrol. 477, 55–71.

Pierini, N.A., Vivoni, E.R., Robles-Morua, A., Scott, R.L. & Nearing, M.A., 2014. Using observations and a distributed hydrologic model to explore runoff thresholds linked with mesquite encroachment in the Sonoran Desert. Water Resour. Res. 50, WR015781.

Qiao, L., Zou, C.B., Will, R.E., Stebler, E., 2015. Calibration of SWAT model for woody plant encroachment using paired experimental watershed data. J. Hydrol. 523, 231–239.

Reedy, R.C., Scanlon, B.R., 2003. Soil water content monitoring using electromagnetic induction. J. Geotech. Geoenvironmental Eng. 129, 1028–1039.

Robinson, D.A., Campbell, C.S., Hopmans, J.W., Hornbuckle, B.K., Jones, S.B., Knight, R., Ogden, F., Selker, J., Wendroth, O., 2008. Soil moisture measurement for ecological and hydrological watershed-scale observatories: A review. Vadose Zone J. 7, 358–389.

Robinson, D.A.L., Ryel, I., Jones, R.J., Scott, B., 2010. Soil water repellency: A method of soil moisture sequestration in pinyon–juniper woodland. Soil Sci. Soc. Am. J. 74, 624–634.

Romme, W.H., Allen, C.D., Bailey, J.D., Baker, W.L., Bestelmeyer, B.T., Brown, P.M., Eisenhart, K.S., Floyd, M.L., Huffman, D.W., Jacobs, B.F., others, 2009. Historical and modern disturbance regimes, stand structures, and landscape dynamics in pinon-juniper vegetation of the western United States. Rangel. Ecol. Manag. 62, 203–222.

Roundy, B.A., Young, K., Cline, N., Hulet, A., Miller, R.F., Tausch, R.J., Chambers, J.C., Rau, B., 2014. Piñon-juniper reduction increases soil water availability of the resource growth pool. Rangel. Ecol. Manag. 67, 495–505.

Ryel, R.J., Ivans, C.Y., Peek, M.S., Leffler, A.J., 2008. Functional Differences in Soil Water Pools: a New Perspective on Plant Water Use in Water-Limited Ecosystems. In Progress in Botany. U. Lüttge, W. Beyschlag, and J. Murata, editors. Springer Berlin Heidelberg, Berlin, Heidelberg. 397–422.

Sala, O.E., Golluscio, R.A., Lauenroth, W.K., Soriano, A., 1989. Resource Partitioning between Shrubs and Grasses in the Patagonian Steppe. Oecologia. 81, 501–505.

Schaap, M.G., Leij, F.J., van Genuchten, M.T., 2001. ROSETTA: a computer program for estimating soil hydraulic parameters with hierarchical pedotransfer functions. J. Hydrol. 251, 163–176.

Schwinning, S., Sala, O., 2004. Hierarchy of responses to resource pulses in arid and semi-arid ecosystems. Oecologia. 141, 211–220.

Schwinning, S., 2010. The ecohydrology of roots in rocks. Ecohydrology, 3, 238–245.

Seyfried, M.S., Schwinning, S., Walvoord, M.A., Pockman, W.T., Newman, B.D., Jackson, R.B., Phillips, F.M., 2005. Ecohydrological control of deep drainage in arid and semiarid regions. Ecology. 86, 277–287.

Sheets, K.R., Hendrickx, J.M., 1995. Noninvasive soil water content measurement using electromagnetic induction. Water Resour. Res. 31, 2401–2409.

Sherlock, M.D., McDonnell, J.J., 2003. A new tool for hillslope hydrologists: spatially distributed groundwater level and soilwater content measured using electromagnetic induction. Hydrol. Process. 17, 1965–1977.

Taucer, P.I., 2006. The effects of juniper removal on rainfall partitioning in the Edwards Aquifer region: large-scale rainfall simulation experiments. Texas A&M University.

Tausch, R.J., West, N.E., Nabi, A.A., 1981. Tree age and dominance patterns in Great Basin pinyon-juniper woodlands. J. Range Manag. 34, 259–264.

Triantafilis, J., Huckel, A.I., Odeh, I.O.A., 2001. Comparison of statistical prediction methods for estimating field-scale clay content using different combinations of ancillary variables. Soil Sci. 166, 415–427.

Triantafilis, J., Lesch, S.M., 2005. Mapping clay content variation using electromagnetic induction techniques. Comput. Electron. Agric. 46, 203–237.

Tromp-van Meerveld, H.J., McDonnell, J.J., 2009. Assessment of multi-frequency electromagnetic induction for determining soil moisture patterns at the hillslope scale. J. Hydrol. 368, 56–67.

Walker, B.H., Noy-Meir, I., 1982. Aspects of the stability and resilience of savanna ecosystems. In Ecology of tropical savannas. Springer. 556–590.

West, A.G., Hultine, K.R., Burtch, K.G., Ehleringer, J.R., 2007. Seasonal variations in moisture use in a piñon–juniper woodland. Oecologia. 153, 787–798.

Western, A.W., Grayson, R.B., Blöschl, G., Willgoose, G.R., McMahon, T.A., 1999. Observed spatial organization of soil moisture and its relation to terrain indices. Water Resour. Res. 35, 797–810.

Wilcox, B.P., Huang, Y., 2010. Woody plant encroachment paradox: Rivers rebound as degraded grasslands convert to woodlands. Geophys. Res. Lett. 37, L07402.

Wilcoxon, F., Wilcox, R.A., 1964. Some rapid approximate statistical procedures. Lederle Laboratories.

Winstral, A., Marks, D., Gurney, R., 2009. An efficient method for distributing wind speeds over heterogeneous terrain. Hydrol. Process. 23, 2526–2535.

Young, J.A., Evans, R.A., Easi, D.A., 1984. Stem flow on western juniper (*Juniperus occidentalis*) trees. Weed Sci. 32, 320–327.

Zégre, N., Skaugset, A.E., Som, N.A., McDonnell, J.J., Ganio, L.M., 2010. In lieu of the paired catchment approach: Hydrologic model change detection at the catchment scale. Water Resour. Res. 46, W11544.

Zhou, Q.Y., Shimada, J., Sato, A., 2001. Three-dimensional spatial and temporal monitoring of soil water content using electrical resistivity tomography. Water Resour. Res. 37, 273–285.

Zou, C.B., Turton, D.J., Will, R.E., Engle, D.M., Fuhlendorf, S.D., 2014. Alteration of hydrological processes and streamflow with juniper (*Juniperus virginiana*) encroachment in a mesic grassland catchment. Hydrol. Process. 28, 6173–6182.

Figure Captions

Figure 1: Aerial photo of study site with elevation contours in meters (black lines), trees with soil moisture probes (blue dots), climate station (yellow triangle), soil sample locations (orange squares) and ERT transect (dotted red line). The map area is the approximate boundary for the EMI survey. The "0" point of the ERT transect is on the east (right) side of the transect.

Figure 2: This figure contains A) snow depth and precipitation per day, volumetric water content at 15 cm (θ_{15}) and 60 (θ_{60}) cm soil depth measured at under the canopy and in the interspace at two trees in the B) low density juniper and C) high density juniper. These θ data are an average for both trees in each density area. Red (orange) arrows indicate when EMI (ERT) surveys occurred.

Figures 3: Plot of change in volumetric water content (Δθ) at 15 cm (A) and 60 cm (B) after rain events plotted against total event precipitation, colored with average event rainfall intensity.

Figures 4: Difference in the change in volumetric water content at 15 cm ($\Delta\theta_{15}$) between tree and interspace after a single rain event. Paired tree and interspace θ_{15} measurements are at the same tree. Tertiles of total event precipitation plotted on the x-axis. For events with values above y = 0, increase in θ_{15} was greater under the tree. Events with values below y = 0, increase in θ_{15} was greater in the interspace. Green (brown) boxplots indicate high juniper/low sagebrush (low juniper/high sagebrush) plot areas, respectively. A non-parametric ANOVA revealed that for precipitation events larger than 1.8 mm, low and high juniper are statistically different.

Figures 5: Regression tree for A) $\Delta\theta_{15}$ and B) $\Delta\theta_{60}$ after a rain event, across total precipitation (P_G), event intensity (P_{int}), vapor pressure deficit (VPD), antecedent soil moisture (θ_{ant}), specific tree, juniper density (low or high), and location (interspace or canopy). Regression tree branches are uniform for improved visibility.

Figure 6: Histograms of soil apparent electrical conductivity (EC_a) data for both A) EMI_{0-75} and B) EMI_{0-150} across May, June, August, and September.

Figure 7: Scatterplot matrix of soil apparent electrical conductivity (EC_a) for A) EMI_{0-75} (0 – 75 cm) and B) EMI_{0-150} (0 – 150 cm) and electrical conductivity of the soil solution (EC_e), volumetric water content (θ), sand, clay, and rock content. The coefficient of determination is in upper panels with size of that number corresponding to coefficient to determination. The scatterplots are fit with a locally weighted linear regression trendline.

Figure 8: Maps EMI inversions for EMI_{0-75} (0 – 75 cm) and EMI_{0-150} (0 – 150 cm) in sequential months from May, June, August, and September.

Figure 9: Absolute (A) and percent change (B) in EC_a, both normalized (divided by) the earlier EC_a survey. Tree canopy height plotted in the background.

Figure 10: Relationship between the max canopy height of adjacent cells and change in the natural log EC_a from August to September. Error bars are 1 standard deviation. Red line is linear regression trend line between the two variables.

Figure 11: This figure shows A) tree location and diameter as well as sagebrush density along the ERT transect, B) inversions of seismic data, C) inversion from ERT survey in May 2014, D) inversion from ERT survey in August 2013, and E) change in resistivity from ERT inversions from May (wet) to August (dry) data.

Figure 12: Change in ERT between May and August, with contour lines delineating the soil – saprolite layer (brown line) and the saprolite – weathered bedrock layer (black line). For juniper canopy and trunk (green triangles and brown rectangles) and sagebrush canopy and trunk (teal asterisk and brown "x"), both the canopy height and diameter are plotted approximately to scale. All juniper within 5 m of the ERT transect are plotted.

Figure 13: Change in resistivity at depth across the high density juniper (0 – 35 m along transect) vs. low density juniper (60 – 100 m along transect) areas, B) Vertically averaged change in resistivity vs. cumulative tree height within 5 m of surface.

Figure 14: Conceptual figure of throughfall, infiltration, and water uptake processes between the canopy and interspace in low and high density juniper areas. More throughfall occurs in the interspace due to juniper canopy interception, therefore greater total infiltration occurs in the near surface of the interspace. But due to preferential infiltration and roots providing pathways for preferential flow below the juniper and sagebrush, deeper redistribution occurs in areas with more sagebrush and juniper due to greater root density. Water advances deeper into the soil in the interspace where there are more sagebrush. Water advances deepest below juniper regardless of where it resides (i.e. in high or low density juniper). Juniper also uptake water at deep in the subsurface in the saprolite.

Table Captions

Table 1: Semivariogram parameters for fitted EC_a models for both $EMI_{0\text{-}75}$ and $EMI_{0\text{-}150}$ for each month.

Table 2: Multiple generalized least squares regression coefficients for ΔEC_a models for both $EMI_{0\text{-}75}$ and $EMI_{0\text{-}150}$. Canopy height (canopy_height) is derived from LiDAR data, water holding capacity (WHC) is calculated with a pedotransfer function from interpolated maps of sand and clay, and snow is from interpolated snow surveys.

Table 1

	EMI_{0-75} **(0 – 75 cm)**					EMI_{0-150} **(0 – 150 cm)**				
Month	**Model**	**Nugget**	**Range (m)**	**Sill**	**Kappa**	**Model**	**Nugget**	**Sill**	**Range (m)**	**Kappa**
May	Spherical	0	9.7	0.53	-	Stein	0.03	0.44	19.4	10
June	Spherical	0.06	18.1	0.59	-	Spherical	0.002	0.62	16.1	-
Aug	Stein	0.03	11.4	0.50	10	Stein	0.03	0.54	11.0	10
Sept	Stein	0.02	12.8	0.47	1.1	Stein	0.01	0.48	14.7	1.6

Table 2

ΔEC_a Model	**Variables** – EMI_{0-75} **(0-75 cm)**			**Variables** – EMI_{0-150} **(0-150 cm)**		
	canopy_height	WHC	snow	canopy_height	WHC	snow
May – June	0.009+	0.383***	0.0004	-0.003	0.297***	0.0004
June – August	-0.009+	1.743***	-0.003	-0.004	1.406***	-0.001
August – Sept	0.002	0.101***	0.0008	0.002	0.138***	-0.0004
May – Sept	0.001	2.247***	-0.003*	-0.0003	1.848***	-0.002

+=p<0.1, *=p>0.05, **=p<0.01,***=p<0.001
(listed variables are those that have p-value <0.1)

Figure 1: Aerial photo of study site with elevation contours in meters (black lines), trees with soil moisture probes (blue dots), climate station (yellow triangle), soil sample locations (orange squares) and ERT transect (dotted red line). The map area is the approximate boundary for the EMI survey. The “0” point of the ERT transect is on the east (right) side of the transect.

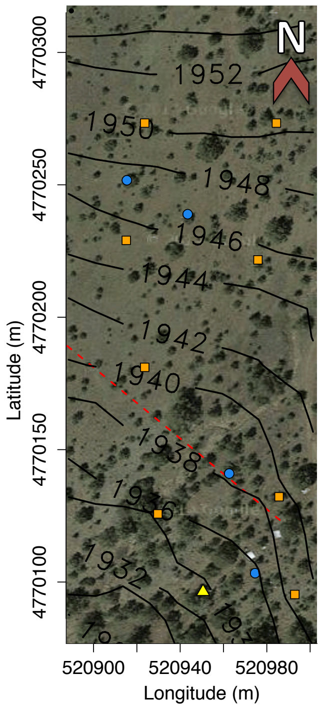

Figure 2: This figure contains A) snow depth and precipitation per day, volumetric water content at 15 cm (θ_{15}) and 60 (θ_{60}) cm soil depth measured at under the canopy and in the interspace at two trees in the B) low density juniper and C) high density juniper. These θ data are an average for both trees in each density area. Red (orange) arrows indicate when EMI (ERT) surveys occurred.

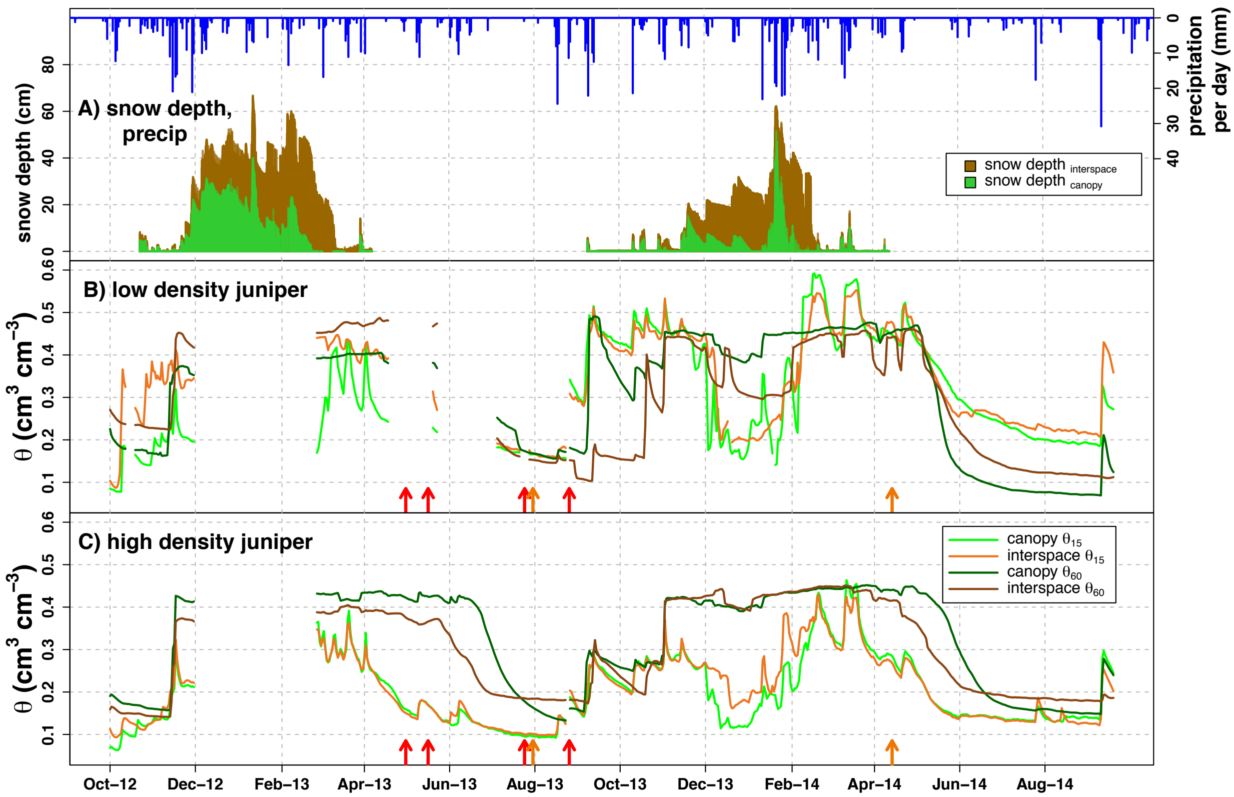

Figure 3: Plot of change in volumetric water content (Δθ) at 15 cm (A) and 60 cm (B) after rain events plotted against total event precipitation, colored with average event rainfall intensity.

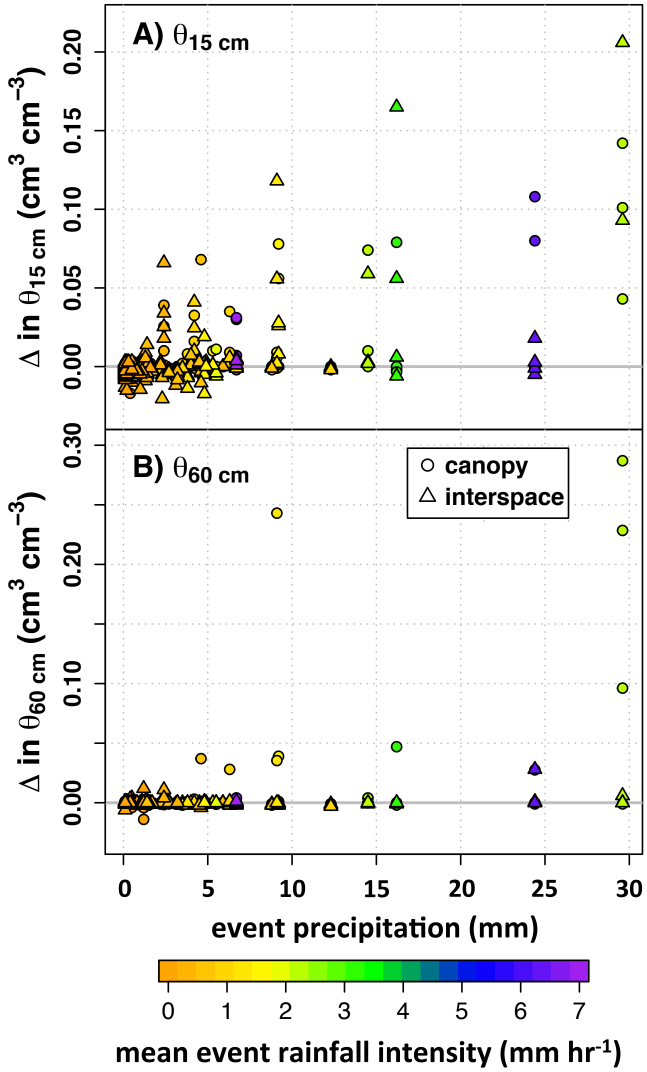

Figure 4: Difference in the change in volumetric water content at 15 cm ($\Delta\theta_{15}$) between tree and interspace after a single rain event. Paired tree and interspace θ_{15} measurements are at the same tree. Tertiles of total event precipitation plotted on the x-axis. For events with values above y = 0, increase in θ_{15} was greater under the tree. Events with values below y = 0, increase in θ_{15} was greater in the interspace. Green (brown) boxplots indicate high juniper/low sagebrush (low juniper/high sagebrush) plot areas, respectively. A non-parametric ANOVA revealed that for precipitation events larger than 5.9 mm, low and high juniper are statistically different.

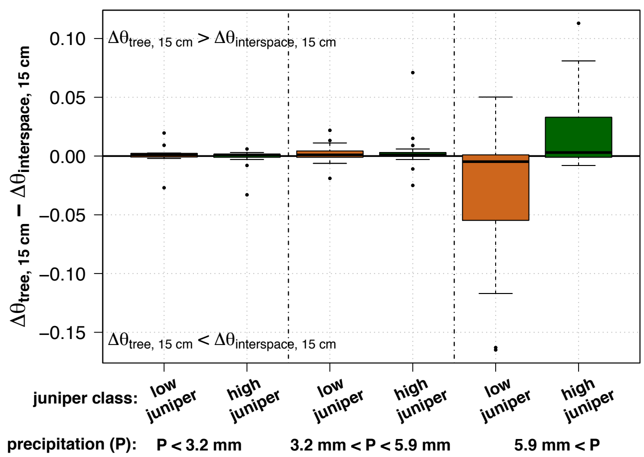

Figure 5: Regression tree for A) $\Delta\theta_{15}$ and B) $\Delta\theta_{60}$ after a rain event, across total precipitaiotn (P_G), event intensity (P_{int}), vapor pressure deficit (VPD), antecedent soil moisture (θ_{ant}), specific tree, juniper density (low or high), and location (interspace or canopy). Regression tree branches are uniform for improved visibility.

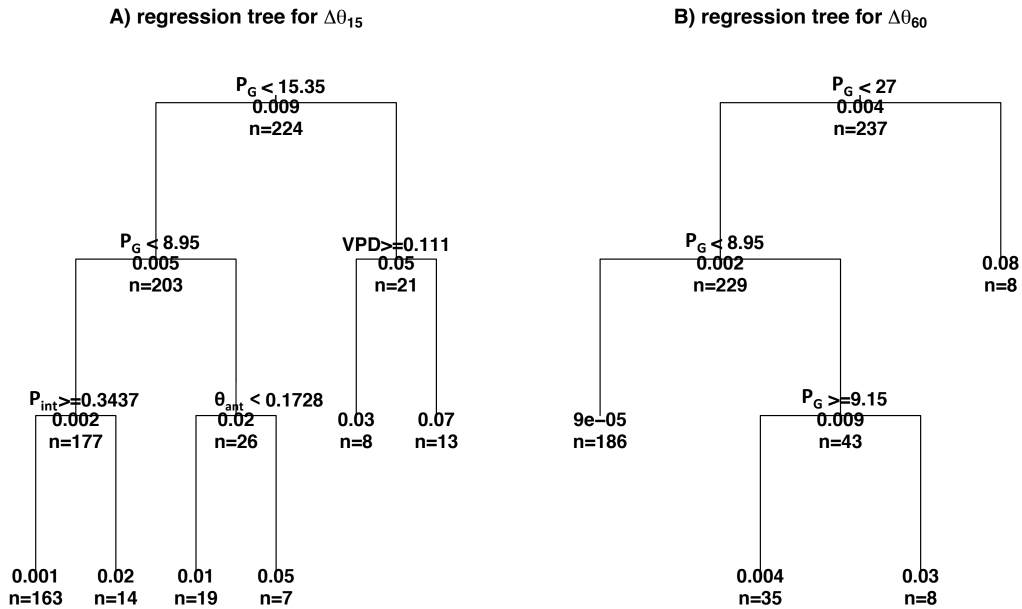

Figure 6: Histograms of EC_a data for both A) $EMI_{0\text{-}75}$ and B) $EMI_{0\text{-}150}$ across May, June, August, and September.

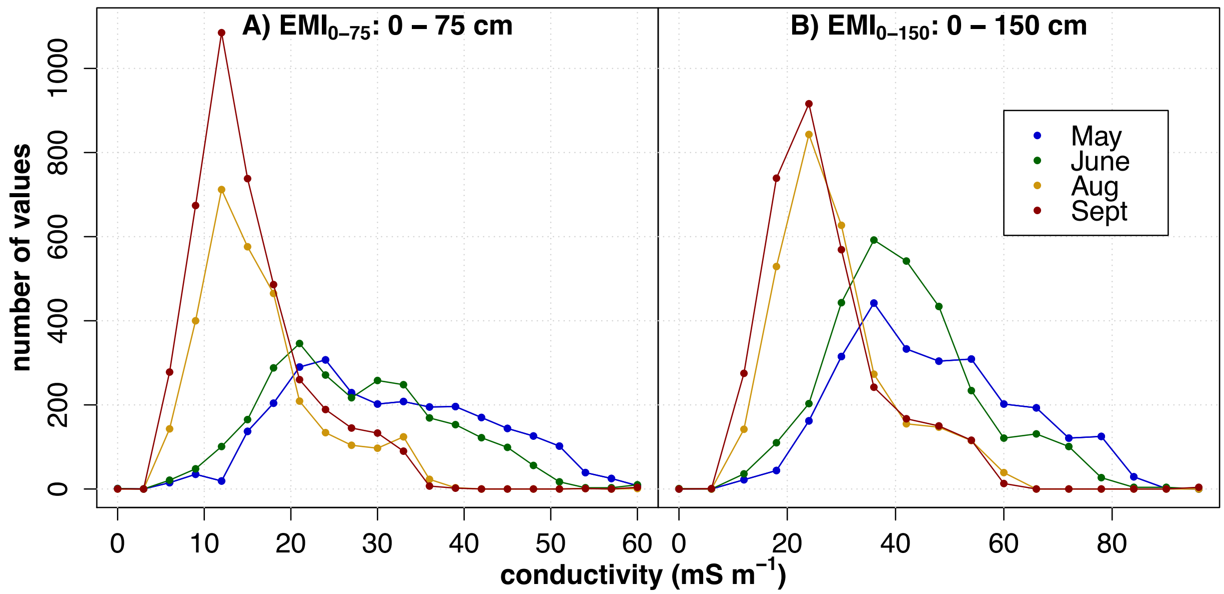

Figure 7: Scatterplot matrix of soil apparent electrical conductivity (EC_a) for A) EMI_{0-75} (0 – 75 cm) and B) EMI_{0-150} (0 – 150 cm) and electrical conductivity of the soil solution (EC_e), volumetric water content (θ), sand, clay, and rock content. The coefficient of determination is in upper panels with size of that number corresponding to coefficient to determination. The scatterplots are fit with a locally weighted linear regression trendline.

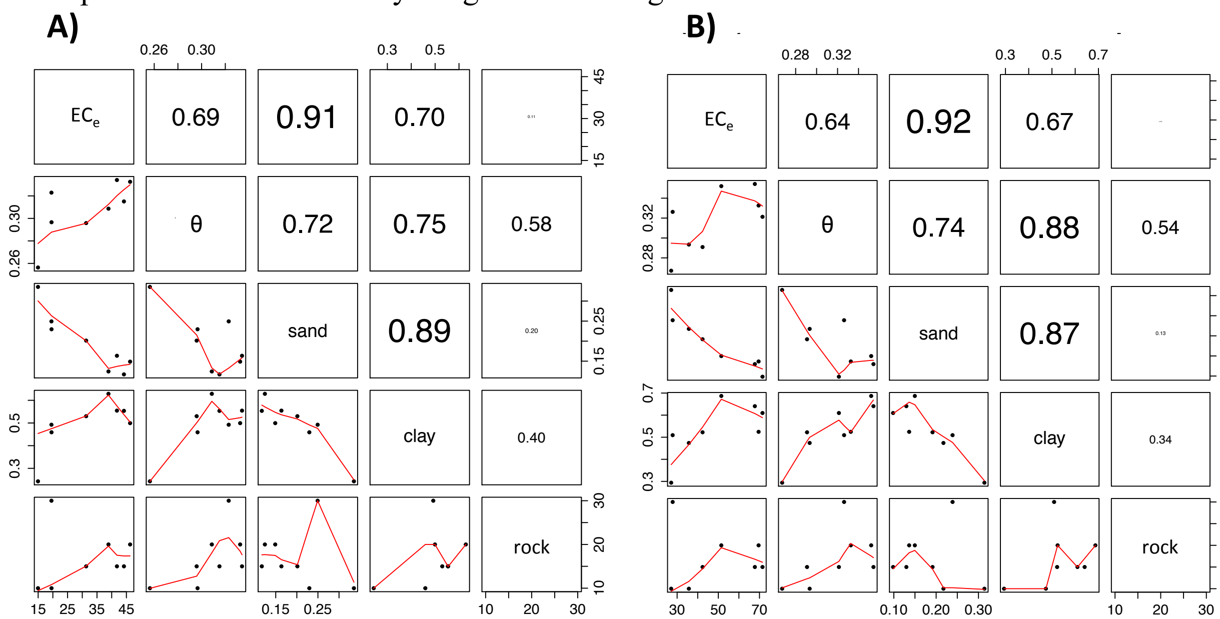

Figure 8: Maps of EMI inversions for $EMI_{0\text{-}75}$ (0 – 75 cm) and $EMI_{0\text{-}150}$ (0 – 150 cm) in sequential months from May, June, August, and September.

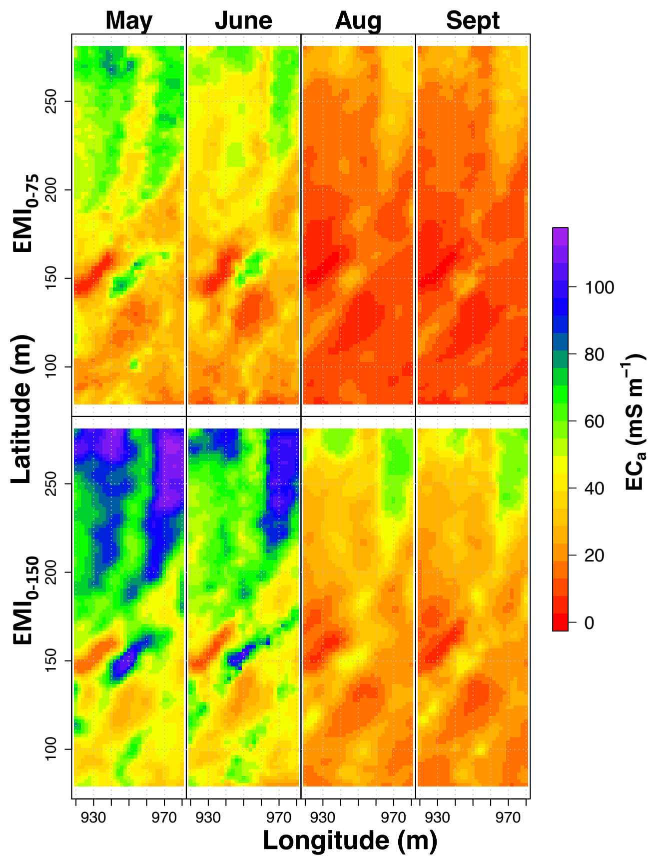

Figure 9: Absolute (A) and percent change (B) in EC_a, both normalized (divided by) the earlier EC_a survey. Tree canopy height plotted in the background.

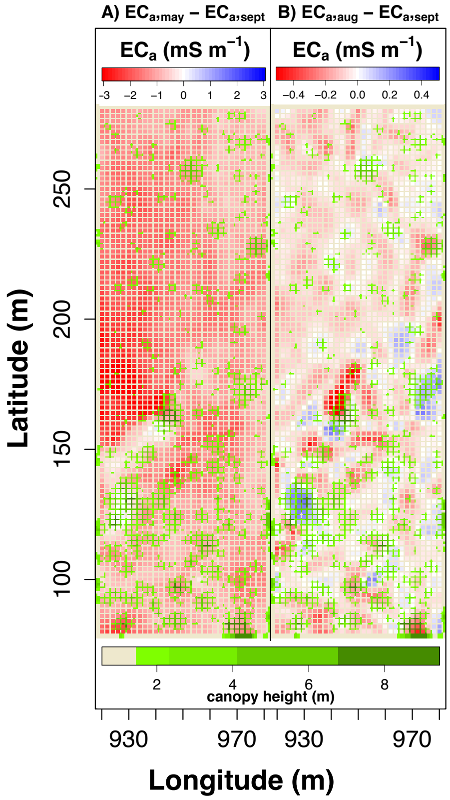

Figure 10: Relationship between the max canopy height of adjacent cells and the natural log of the change in $EMI_{0\text{-}150}$ EC_a from August to September. Error bars are 1 standard deviation. Red line is linear regression trend line between the two variables.

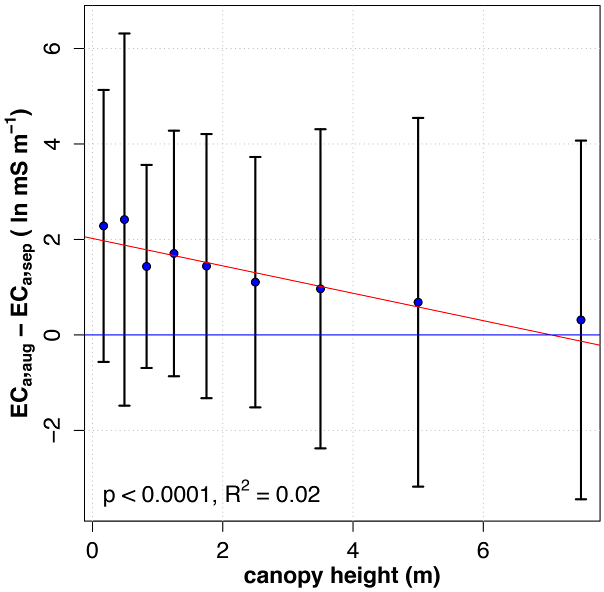

Figure 11: This figure shows A) tree location and diameter as well as sagebrush density along the ERT transect, B) inversions of seismic data, C) inversion from ERT survey in May 2014, D) inversion from ERT survey in August 2013, and E) change in resistivity from ERT inversions from May (wet) to August (dry) data.

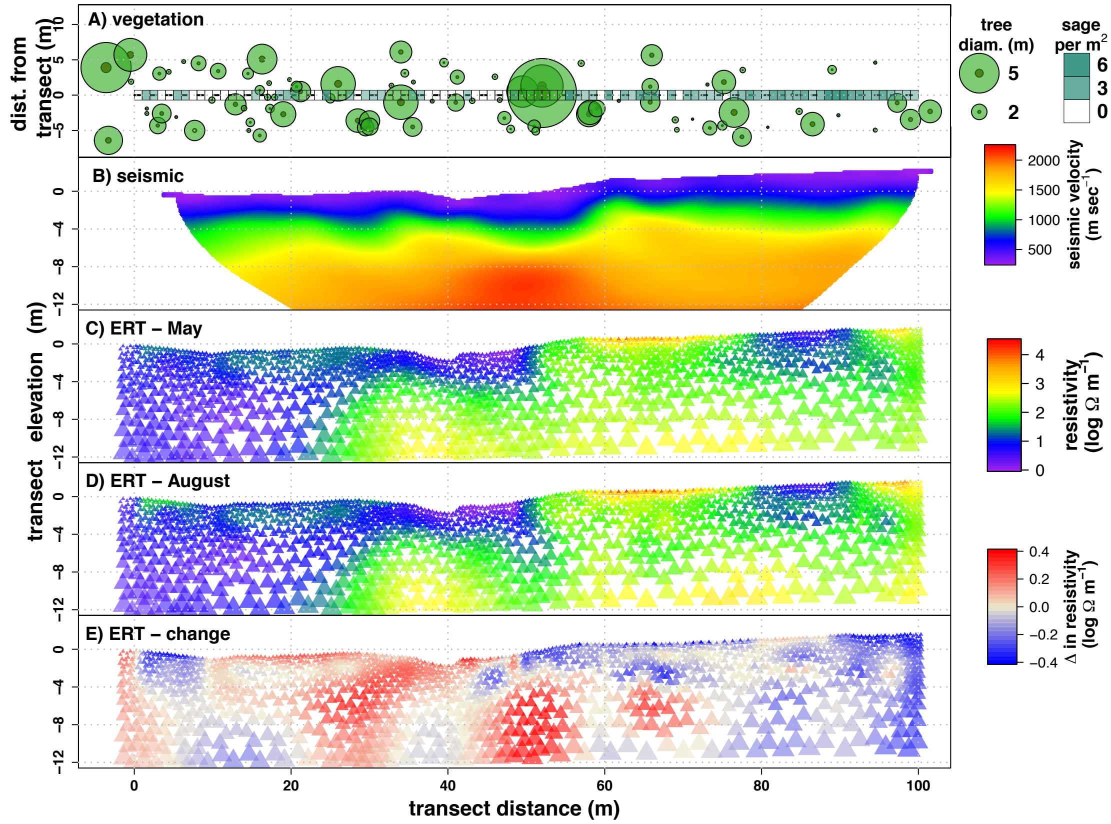

Figure 12: Change in ERT between May and August, with contour lines delineating the soil – saprolite layer (brown line) and the saprolite – weathered bedrock layer (black line). For juniper canopy and trunk (green triangles and brown rectangles) and sagebrush canopy and trunk (teal asterisk and brown "x"), both the canopy height and diameter are plotted approximately to scale. All juniper within 5 m of the ERT transect are plotted.

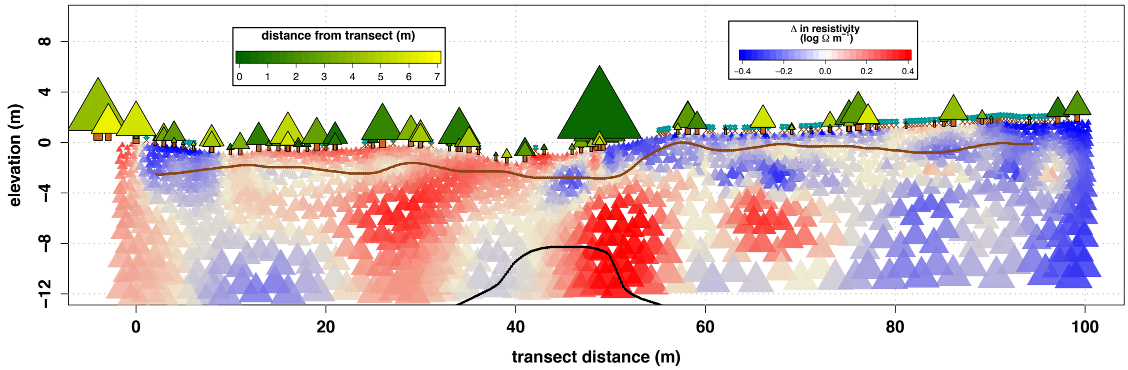

Figure 13: A) Change in resistivity at depth across the high density juniper (0 – 35 m along transect) vs. low density juniper (60 – 100 m along transect) areas, and B) vertically averaged change in resistivity vs. cumulative tree height within 5 m of surface.

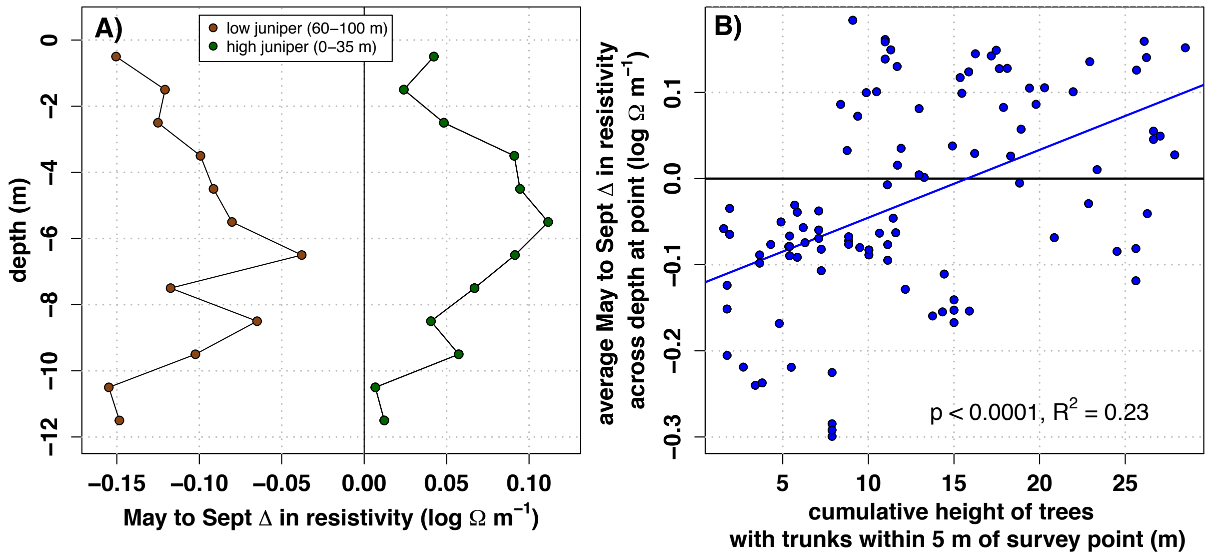

Figure 14: Conceptual figure of throughfall, infiltration, and water uptake processes between the canopy and interspace in low and high density juniper areas. More throughfall occurs in the interspace due to juniper canopy interception, therefore greater total infiltration occurs in the near surface of the interspace. But due preferential infiltration and roots providing pathways for preferential flow below the juniper and sagebrush, deeper infiltration occurs in areas with A) more sagebrush and B) juniper. Infiltration goes deeper in the interspace where there are more sagebrush. Infiltration goes deepest below juniper regardless of where it resides. Juniper also uptake water at deep in the subsurface in the saprolite.